



Numerical Investigation on Hydrogen-Fueled Scramjet Combustor with Parallel Strut Fuel Injector at a Flight Mach Number of 6

K. M. Pandey[†], S. Roga¹ and G. Choubey

Department of Mechanical Engineering, National Institute of Technology Silchar, Assam, India

[†]Corresponding Author Email: kmpandey2001@yahoo.com

(Received September 24, 2014; accepted September 1, 2015)

ABSTRACT

A numerical analysis of the inlet-combustor interaction and flow structure through a scramjet engine at a flight Mach number $M = 6$ with parallel injection (Strut with circular inlet) is presented in the present research article. Three different angles of attack ($\alpha = -4^\circ$, $\alpha = 0^\circ$, $\alpha = 4^\circ$) have been studied for parallel injection. The scramjet configuration used here is a modified version of DLR scramjet model. Fuel is injected at supersonic speed ($M=2$) through a parallel strut injector. For parallel injection, the shape of the strut is chosen in a way to produce strong stream wise vorticity and thus to enhance the hydrogen/air mixing inside the combustor. These numerical simulations are aimed to study the flow structure, supersonic mixing, and combustion phenomena for the three different types of geometries along with circular shaped strut configuration.

Keywords: Scramjet; Hypersonic Combustion; $k-\epsilon$ Realizable model; Parallel injector.

NOMENCLATURE

A	cross section area	x	axial distance
f	fuel-air ratio	Y	mass fraction
K	turbulent kinetic energy	h	height
M	Mach number		
C_y	force coefficient in the y direction	ϵ	turbulent dissipation rate
P	pressure	η	Efficiency parameter
T	temperature	α	angle of attack
U	axial velocity	ϕ	equivalence ratio

1. INTRODUCTION

As the powered flight of X-43 A and X-51A achieved success in the recent years, hydrogen-fueled scramjet engines have become one of the most promising air breathing propulsion technologies in the future access to space and hypersonic flight programs. Due to this, this area has drawn an ever increasing attention of researchers worldwide. For a number of reasons, hydrogen is often considered as the fuel for scramjets for hypersonic vehicles. But delay periods are important part of high speed hypersonic vehicles and information on delay periods for hydrogen-air systems is not plentiful. The work on numerical investigation of a hydrogen-fueled scramjet combustor at flight conditions are done by E.

Rabadan *et al.* (2012, 2013) and their findings are, as the equivalence ratio was increased, the combustion became stronger causing an upstream displacement of the shock train producing different pressure variations. Computational analysis of scram-jet combustor at flight Mach no 7 is done by Pandey *et al.* (2015). They found that the shock relocation inside the combustor improved the burning and diminished the ignition delay Vadim Yu. *et al.* (2010) worked on hypersonic technology development concerning high speed air-breathing engines and they found that small penetration of fuel into supersonic flow causes combustion only near to a wall, large losses of total pressure. K. A. Skinner and R. J. Stalker (1996) worked on species measurements in a hypersonic, hydrogen-air, and combustion wake and found that at lower pressures,

the ignition delay and heat release times will be much greater than the minimum values of 0.5 and 1 ms respectively. J. Swithenbank *et al.* (1996) worked on hypersonic air-breathing propulsion and his findings are chemical rearrangement time for combustion can be large at low temperature and pressures. I. N. Momtchiloff *et al.* (1963) worked on kinetics in hydrogen-air flow systems. And calculations of ignition delays for hypersonic ramjets and their findings are, the ignition delay length increases rapidly at the lower flight Mach numbers. Oldenborg, R.C (1989) worked on critical reaction rates in hypersonic combustion chemistry and found that High Mach number flight also results in very short residence times (millisecond time range) in a hypersonic engine which causes poor chemical combustion efficiency. S. Yungster and K. Radhakrishnan (2001) worked on simulation of unsteady hypersonic combustion around projectiles in an expansion tube and found that the flame propagation produces a series of oblique shock waves that reignite the core flow, creating an oblique detonation wave whose interaction with the laterally expanding boundary layer flame gives rise to a normal detonation wave that propagates. K. Kumaran and V. Babu (2009) worked on investigation of the effect of chemistry models on the numerical predictions of the supersonic combustion of Hydrogen. And their findings are-Multi step chemistry predicts higher and wider spread heat release than what is predicted by single step chemistry. Shigeru Aso *et al.* (2005) worked on fundamental study of supersonic combustion in pure air flow with use of shock tunnel and found that the increase of injection pressure generated strong bow shock, resulting in the pressure loses. The shock generator is an effective method to accelerate the combustion.

Based on these facts, the aim of the present study is to investigate the flame holding and combustion enhancement for three different angle of attack geometries. Different parameters are studied, like temperature, density contour, Mach number distribution, wall pressure and combustion efficiency. It is found that modified scramjet combustors with negative angle of attack have improved the combustion efficiency and it has shorter ignition delay as compared to other two geometries. The $k-\epsilon$ Realizable computational model is capable of predicting flow simulations well and good.

2. GOVERNING EQUATIONS

The Standard $k-\epsilon$ is a well-established model capable of resolving through the boundary layer. The second model is Realizable $k-\epsilon$, an improvement over the standard $k-\epsilon$ model. It is a relatively recent development and differs from the standard $k-\epsilon$ model in two ways. The realizable $k-\epsilon$ model contains a new formulation for the turbulent viscosity and a new transport equation for the dissipation rate, ϵ that is derived from an exact equation for the transport of the mean-square vorticity fluctuation. Neither the standard $k-\epsilon$

model nor the RNG $k-\epsilon$ model is realizable. It introduces a Variable C_μ instead of constant.

Continuity:

$$\frac{\partial \rho}{\partial t} + \frac{\partial(\rho u)}{\partial x} + \frac{\partial(\rho v)}{\partial y} + \frac{\partial(\rho w)}{\partial z} = 0 \quad (1)$$

X momentum:

$$\frac{\partial(\rho u)}{\partial t} + \frac{\partial(\rho uu)}{\partial x} + \frac{\partial(\rho uv)}{\partial y} + \frac{\partial(\rho uw)}{\partial z} = \frac{\partial \sigma_{xx}}{\partial x} + \frac{\partial \tau_{yx}}{\partial y} + \frac{\partial \tau_{zx}}{\partial z} \quad (2)$$

Y momentum:

$$\frac{\partial(\rho v)}{\partial t} + \frac{\partial(\rho uv)}{\partial x} + \frac{\partial(\rho vv)}{\partial y} + \frac{\partial(\rho vw)}{\partial z} = \frac{\partial \sigma_{yy}}{\partial y} + \frac{\partial \tau_{xy}}{\partial x} + \frac{\partial \tau_{zy}}{\partial z} \quad (3)$$

Z momentum:

$$\frac{\partial(\rho w)}{\partial t} + \frac{\partial(\rho uw)}{\partial x} + \frac{\partial(\rho vw)}{\partial y} + \frac{\partial(\rho ww)}{\partial z} = \frac{\partial \sigma_{zz}}{\partial z} + \frac{\partial \tau_{xz}}{\partial x} + \frac{\partial \tau_{yz}}{\partial y} \quad (4)$$

Transport Equations

$$\frac{\partial}{\partial t}(\rho k) + \frac{\partial}{\partial x_j}(\rho k u_j) = \frac{\partial}{\partial x_j} \left[\left(\mu + \frac{\mu_t}{\sigma_k} \right) \frac{\partial k}{\partial x_j} \right] + P_k + P_b - \rho \epsilon - Y_M + S_k \quad (5)$$

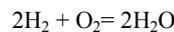
$$\frac{\partial}{\partial t}(\rho \epsilon) + \frac{\partial}{\partial x_j}(\rho \epsilon u_j) = \frac{\partial}{\partial x_j} \left[\left(\mu + \frac{\mu_t}{\sigma_\epsilon} \right) \frac{\partial \epsilon}{\partial x_j} \right] + \rho C_1 S_\epsilon - \rho C_2 \frac{\epsilon^2}{k + \sqrt{k \epsilon}} + C_{3\epsilon} \frac{\epsilon}{k} C_{3\epsilon} P_b + S_\epsilon \quad (6)$$

Where

$$C_1 = \max \left[0.43, \frac{\eta}{\eta + 5} \right], \eta = S \frac{k}{\epsilon}, S = \sqrt{2 S_{ij} S_{ij}}$$

Combustion modeling

The most common combustion modelling approach and also one used in this research work is the finite rate/eddy dissipation model Single step chemistry model is taken to find the flow physics phenomenon inside the combustor at hypersonic condition. The reaction used for the Scramjet was the hydrogen-water reaction:



2.1 The Scramjet Combustor

A schematic of the DLR (German Aerospace centre) scramjet experimental facility, (1994, 1995, 1996), is presented in Fig. 1 which is taken for the purpose of validation only. In our work we used models which are different from Waidmann *et al.* (1994, 1995, and 1996). The length of the scramjet is 500 mm with a constant cross-section width of 65mm and maximum height of 71 mm. The strut injector is located at axial position $x = 140$ mm. Hydrogen fuel (H_2) is injected parallel to the air stream at $M = 2$ through a row of 15 holes of the strut each with a diameter of 1 mm and 2.4 mm apart from each other in the strut base where as air stream enters the combustor at $M=6$. The combustor section has a width of 65 mm and a height of 60 mm at the entrance. The Schematic diagram of DLR supersonic combustion chamber (1994, 1995, 1996)

And modified scramjet combustor with $\alpha=0^\circ$ angle of attack is shown in Fig 1 and 2.

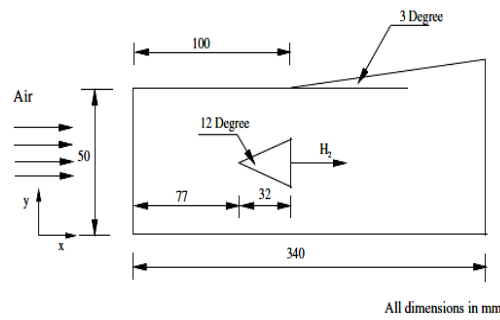
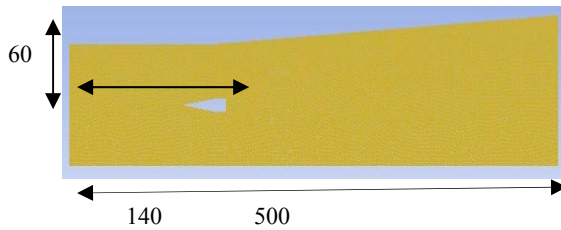


Fig. 1. Schematic diagram of DLR supersonic combustion chamber (1994, 1995, 1996).



All dimensions are in mm

Fig. 2. Modified scramjet combustor with $\alpha=0^\circ$ angle of attack.

2.2 Mesh Generation

To reduce the computational time as much as possible, but still retaining all relevant physics of the scramjet combustor, the computational configuration is simplified in the sense that all the meshing, modeling and computational analyses are done in 2D. In the present case all the 2D models are generated using Icem-CFD and computational analysis are done by using Ansys 14-Fluent commercial software (2011). For all the geometries, 2D, unstructured quadrilateral grids are generated as given in fig 3.

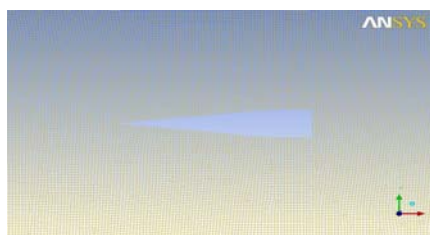


Fig. 3. Mesh generation in scramjet combustor for $\alpha=0^\circ$ angle of attack.

2.3 Grid Convergence Test

Here grid independence test is carried out to analyze the effect of grid number on the maximum static temperature of the flow field. After refinement a grid with 272136 element for circular shaped injector have been taken as final grid for all subsequent calculations.

2.4 Boundary Condition

Three types of boundaries are applied: inflow, outflow and fixed walls and the entire flow field is

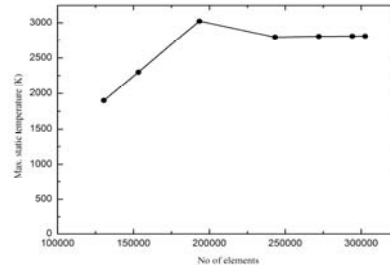


Fig. 6. Grid Independence Test for the strut with circular inlet.

considered to be supersonic. Dirichlet boundary conditions are applied for variables at inflow and Neumann boundary conditions are used for all variables at outflow. Also no slip condition is applied on fixed walls. The computations are all initialized with the state of incoming air

Table 1 Inflow conditions of the incoming air stream and hydrogen jet for air Mach number 6 and H₂ Mach number 2

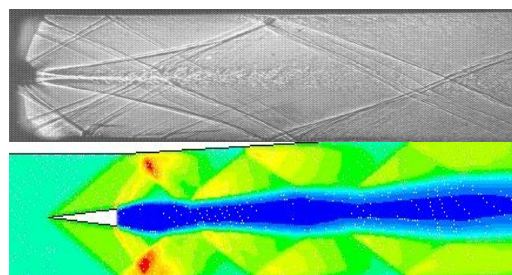
S. No	variables	Air	Hydrogen
1	Ma	6	2
2	T(k)	800	300
3	P(Pa)	5000	5000
5	Y _{O₂}	0.232	0
6	Y _{N₂}	0.736	0
7	Y _{H₂O}	0.032	0
8	Y _{H₂}	0	1

3. RESULTS AND DISCUSSIONS

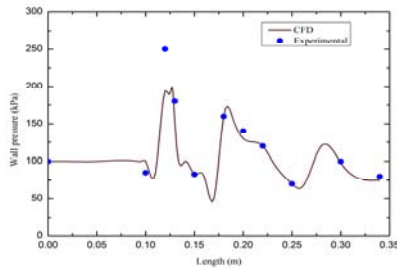
All simulations are started with the state of incoming air.

3.1 Validation of CFD Work

For parallel injection, fig.7 shows a view of the flow together with a qualitative comparison of experimental shadowgraph images and numerical images for the cases of H₂ injection. With H₂ injection, oblique shocks are formed at the tip of the wedge that is later reflected by the upper and lower walls. At the upper and lower walls, the boundary layer is affected by the reflected oblique shocks. In some places the reflected shock waves are deflected by the hydrogen jets. Wall pressure distribution for single strut with $\alpha=0^\circ$ angle of attack as shown in fig 7(b) have good agreement with the DLR experimental results reported in Oevermann (2000)



(a)



(b)
Fig. 7. (a) Experimental shadowgraph (Schlieren image of hydrogen injection) and contour plot of density (b) Wall pressure distributions for single-strut experimentally and with CFD simulations. (2000).

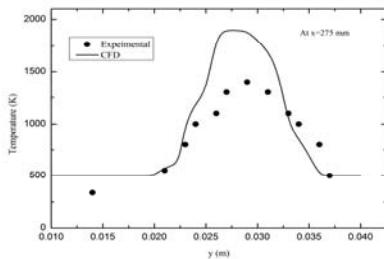


Fig. 8. Temperature at $x = 275$ mm for single-strut experimentally and with CFD simulations (1995).

Fig.8 also represents temperature distribution at $x = 275$ mm for single-strut experimentally (1995) and with CFD simulations for $\alpha=0^\circ$. Between the experimental and computational result, reasonable agreement is found, with a slightly higher peak temperature for computational case.

3.2 Air Mach no=6, Hydrogen Mach no=2

Fig. 9 shows the temperature distribution for the investigated angles of attack. The heat addition in the combustor helps in changing both the static temperature and the flow velocity. As a result, it is reflected in an increase of total temperature. The presence of chemical kinetics and chemical equilibrium of heat release depends on the static temperature. Hydrogen is transported and mixed with the surrounding flow due to the stream wise vorticity induced by the circular strut injector. After hydrogen is mixed with air stream, there is sudden increase in pressure and temperature which are enough for auto ignition and then combustion starts.

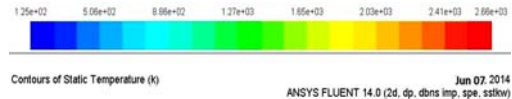
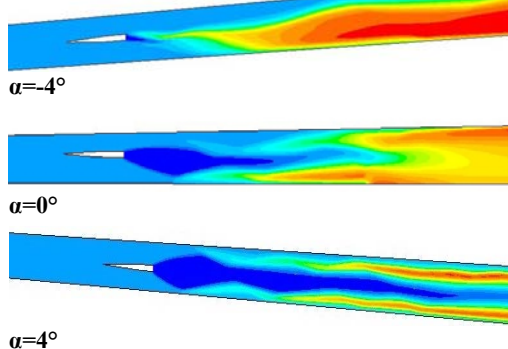


Fig. 9. Temperature distribution for different angle of attack [$\alpha=-4^\circ, \alpha=0^\circ, \alpha=4^\circ$] for $M=6$.

The generation and strength of the vortices depends mainly on the injector's geometry. The ignition delay is affected by the variation of the angle of attack. The shortest ignition delay is observed for the configuration with $\alpha=-4^\circ$ while the longest ignition delay appears for $\alpha=4^\circ$. The highest temperature is registered for a negative angle of attack $\alpha=-4^\circ$ approximately $T_{max} = 2600K$. For the configuration with an angle of attack $\alpha=-4^\circ$, the increase in temperature takes place approximately 30 mm downstream of the injection. For the configuration with $\alpha=0^\circ, \alpha=4^\circ$ the ignition delay is approximately 70 mm and 85 mm.

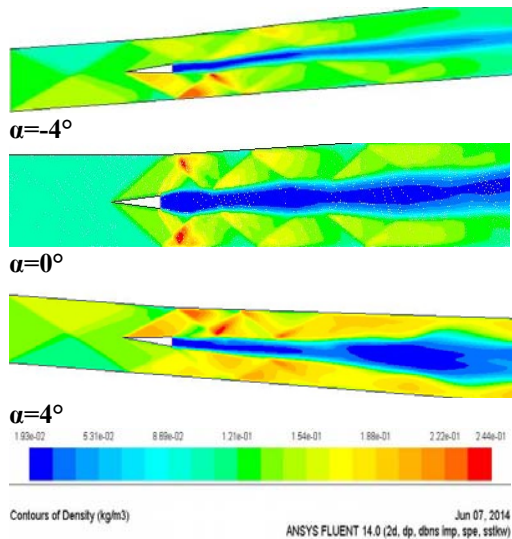


Fig. 10. Density distribution for different angle of attack [$\alpha=-4^\circ, \alpha=0^\circ, \alpha=4^\circ$] for $M=6$.

Fig.10 represents the contour of density for different angle of attack. Here with H_2 injection, oblique shocks are formed at the tip of the wedge that is later reflected by the upper and lower walls. At the upper and lower walls, the boundary layer is affected by the reflected oblique shocks. In some places the reflected shock waves are deflected by the hydrogen jets. The boundary layer on the wedge surface separates at the base and a shear layer is formed. This shear layer is naturally unstable and is therefore prone to break-up. Because of the one-sided divergent channel the upper reflecting shock hits the H_2 filled wake further downstream than the lower shock. In some places the reflected shock waves are deflected by the hydrogen jets. After some distance the flow in the wake of the wedge is accelerated back to supersonic speed. A small triangular recirculation region is formed just behind the wedge caused by low velocity.

Fig. 11 shows variation of the Mach number for three different geometries of scramjet combustor at the different level, at the entrance the air Mach no is

6, at the base of the circular strut the hydrogen is injected at Mach no 2. For all the geometries, in the middle of the chamber the Mach number values are reduced to below 2. It happened due to shape of the Strut and interaction of different waves.

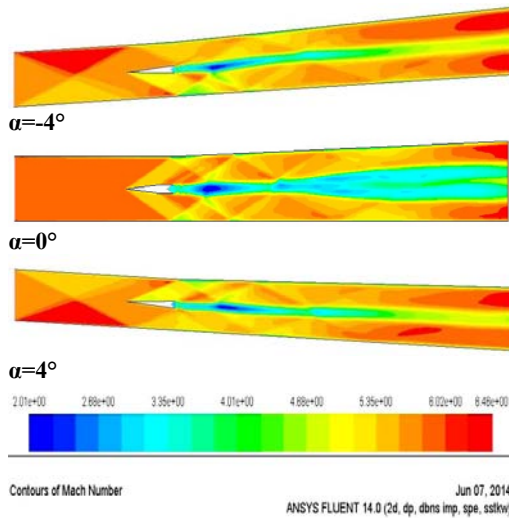


Fig. 11. Computed Mach number distribution for different angles of attack (α) for $M=6$.

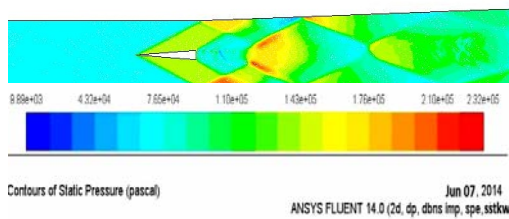


Fig. 12. Computed pressure distribution for $\alpha=0^\circ$ angles of attack.

Fig. 12 represents the computed pressure distribution for $\alpha=0^\circ$ angle of attack where at the leading edge of the circular strut injector a shock is formed. This shock travels downstream and is deflected at the top and bottom wall. The shock loses its intensity as its travels towards the outlet.

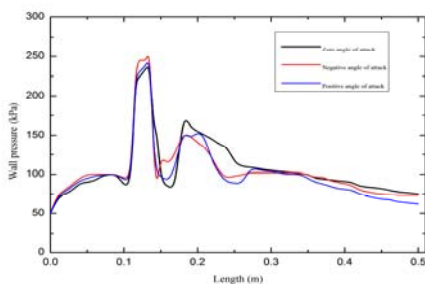


Fig. 13. Computed wall pressure distribution at the top wall for different angle of attack. [$M=6$].

Fig. 13 shows the computed wall pressure distribution at the top wall for different angle of attack ($M=6$). The highest pressure peak at the top wall is registered at approx. $X=120\text{mm}$ with a corresponding pressure $p=250\text{kPa}$. This maximum value is observed for $\alpha=-4^\circ$ i.e. for negative angle of attack.

4. PERFORMANCE MEASURES

A useful parameter to identify the combustor performance is the combustion efficiency.

4.1 Combustion Efficiency

The combustion efficiency η_{comb} represents how much of the hydrogen has been burned in a given cross section (A_x) with respect to the total injected hydrogen. The combustion efficiency is defined by Gerlinger (2008) as:

$$\eta_{comb}(x) = 1 - \frac{\int A(x) \rho_{gas} u Y_{H_2} dA}{\dot{m}_{H_2inj}} \quad (7)$$

Where ρ is the gas density, Y_{H_2} is the mass fraction of hydrogen, \dot{m}_{H_2inj} is the injected hydrogen

mass flux, and u is the velocity component normal to the cross section. The combustion efficiency is presented in fig 14. The plot starts right after the trailing edge of the circular strut injector ($x = 140\text{mm}$) since no hydrogen is available in upstream direction. The ignition of the fuel-air mixture takes place downstream of the trailing edge of the injector. The combustion efficiency grows near the injection region where hydrogen is rapidly mixed due to the strong stream wise vorticity. For high equivalence ratios, the combustion efficiency decreases as a consequence of the decrease in the mixing efficiency due to high values of hydrogen mass flow. As the vortices travel downstream, they become weak and their ability to spread the fuel into the surrounding flow decreases. This leads to a decrease in mixing and consequently in combustion efficiency as the mixing is not sufficient. In present case the highest combustion efficiency is observed for three struts injection system (approx 88%) as compared to two struts (70%) as well as single strut injection (44%) system

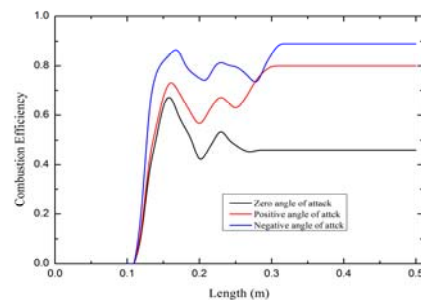


Fig. 14. Computed combustion efficiency for different angles of attack. [$M=6$].

5. CONCLUSION

In this research work, $k-\epsilon$ Realizable computational turbulence model, the finite rate/eddy-dissipation reaction model and single step chemistry are employed to simulate the hypersonic flow field of the hydrogen fueled scramjet combustor with two types of strut flame holder (strut with circular injector), for three angle of

attack ($\alpha=-4^\circ$, $\alpha=0^\circ$, $\alpha=4^\circ$). Different flow and performance parameters like static wall pressure, temperature, Mach number, and density distribution as well as combustion efficiency were discussed. The following results are obtained:

- It is observed that computational results having a good agreement qualitatively and quantitatively with experiments for $\alpha=0^\circ$ angle of attack
- Again there is no influence of the strut injector in upstream direction towards the isolator was found as that of Rabadan *et al.*
- Shock train is displaced in upstream direction for a negative angle of attack was observed. This shock displacement enhanced the combustion and decreased the ignition delay. This shock modifies the shock pattern in the combustor.
- It was also observed that maximum temperature occurred in the recirculation areas for $\alpha=-4^\circ$ approx. 2600 K as compared to $\alpha=0^\circ$ and $\alpha=4^\circ$. The ignition delay is also found to be shorter for $\alpha=-4^\circ$
- Combustion efficiency is found to be highest (approx. 88%) in case of $\alpha=-4^\circ$ as compared to $\alpha=0^\circ$ and $\alpha=4^\circ$.

REFERENCES

- Aleksandrov, V. Y., A. N. Prokhorov and V. L. Semenov (2010). Hypersonic technology development concerning high speed air-breathing engines. *Presented at the 10th International Congress of Fluid Dynamics*, Ain Soukhna, Red Sea, Egypt, December 16–19, 1–15.
- ANSYS. ANSYS Fluent 14.0 theory guide, Canonsburg, PA 15317, ANSYS, Inc. 2011
- Aso, S., A. Hakim, S. Miyamoto, K. Inoue and Y. Tani (2005). Fundamental study of supersonic combustion in pure air flow with use of shock tunnel. *Acta Astronautica* 57, 384–389
- Gerlinger, P., P. Stoll, M. Kindler, F. Schneider and M. Aigner (2008). Numerical investigation of Mixing and Combustion Enhancement in Supersonic Combustors by Strut Induced Streamwise Vorticity, *Aerospace Science and Technology* ELSEVIER 12, 159-68 .
- Momtchiloff, I. N., E. D. Taback and R. F. Buswell (1963). Kinetics in hydrogen-air flow systems. I. Calculation of ignition delays for hypersonic ramjets. *Symp. (Int.) Combustion* 9, 220–230.
- Oldenberg, R. C., D. M. Harradine, G. W. Loge, J. L. Lyman, G. L. Schott and K. R. Winn (1989). Critical reaction rates in hypersonic combustion chemistry. *Presented at the American Chemical Society national meeting*, Miami, FL, September 10–15. Report no, LA-UR-89-2170, Los Alamos National Laboratory.
- Pandey, K. M., S. Roga and G. Choubey (2015). Computational Analysis of Hypersonic Combustor Using Strut Injector at Flight Mach 7, *Combustion Science and Technology*, 187(9), 1392-1407.
- Rabadan Santana, E. and B. Weigand (2012). Numerical Investigation of Inlet Combustor Interactions for a Scramjet Hydrogen-Fueled Engine at a Flight Mach number of 8. *18th AIAA/3AF International Space Planes and Hypersonic Systems and Technologies Conference, Tours, France*, Paper ID AIAA-2012-5926, DOI: 10.2514/6.2012-5926
- Rabadan, E. and B. Weigand (2013). Numerical Investigation of a Hydrogen-fueled Scramjet Combustor at Flight Conditions, *EUCASS Book Series: Progress in Propulsion Physics* 4, 373-394, ISBN 978-2-7598-0876-2.
- Skinner, K. A. and R. J. Stalker (1996). Species measurements in a hypersonic, hydrogen-air, combustion wake. *Combustion Flame* 106, 478–486.
- Swithenbank, J. (1966). Hypersonic air-breathing propulsion. *In Progress in Aeronautical Sciences*, 8, Pergamon Press.
- Waidmann, W., F. Alff, M. Bohm, U. Brummund W. Clauss and M. Oswald (1994). Experimental investigation of hydrogen combustion process in a supersonic combustion ramjet (SCRAMJET) □ DGLR, Jahrestagung, Erlangen, Germany 629–638.
- Waidmann, W., F. Alff, M. Bohm, U. Brummund, W. Clauss and M. Oswald (1995). Supersonic combustion of hydrogen- air in a scramjet combustion chamber. □ *Space Technol.* 15(6), 421–429. 1995
- Waidmann, W., U. Brummund and J. Nuding (1996). Experimental investigation of supersonic ramjet combustion (Scramjet). *8th Int. Symp. On Transport Phenomena in Combustion*, Taylor & Francis, Boca Raton, FL. 1996
- Yungster, S. and K. Radhakrishnan (2001). Simulation of Unsteady Hypersonic Combustion around Projectiles in an Expansion Tube, vol. 11, *Institute for Computational Mechanics in Propulsion, NASA Glenn Research Center, Cleveland, OH*, 1–12. Kumaran, K., and Babu, V. (2009) Investigation of the effect of chemistry models on the numerical predictions of the supersonic combustion of hydrogen. *Combustion and Flame* 156, 826–841